ChemPubSoc Europe
DOI: 10.1002/chem.201402426
CHEMISTRY
A European Journal
Full Paper

Helicenes

Formation of One-Dimensional Helical Columns and Excimerlike Excited States by Racemic Quinoxaline-Fused [7]Carbohelicenes in the Crystal

Hayato Sakai,*[a] Sho Shinto,[a] Yasuyuki Araki,*[b] Takehiko Wada,[b] Tomo Sakanoue,[c] Taishi Takenobu,*[c] and Taku Hasobe*[a]

Abstract: A series of quinoxaline-fused [7]carbohelicenes (HeQu derivatives) was designed and synthesized to evaluate their structural and photophysical properties in the crystal state. The quinoxaline units were expected to enhance the light-emitting properties and to control the packing structures in the crystal. The electrochemical and spectroscopic properties and excited-state dynamics of these compounds were investigated in detail. The first oxidation potentials of HeQu derivatives are approximately the same as that of unsubstituted reference [7]carbohelicene (Heli), whereas their first reduction potentials are shifted to the positive by about 0.7 V. The steady-state absorption, fluorescence, and circular dichroism spectra also became redshifted compared to those of Heli. The molecular orbitals and energy levels of the HOMO and LUMO states, calculated by DFT methods, support these trends. Moreover, the absolute fluorescence quantum yields of HeQu derivatives are about four times larger than that of Heli. The structural properties of the aggregated states were analyzed by single-crystal analysis. Introduction of appropriate substituents (i.e., 4-methoxyphenyl) in the HeQu unit enabled the construction of one-dimensional helical columns of racemic HeQu derivatives in the crystal state. Helix formation is based on intracolumn π-stacking between two neighboring [7]carbohelicenes and intercolumn CH⋅⋅⋅N interaction between a nitrogen atom of a quinoxaline unit and a hydrogen atom of a helicene unit. The time-resolved fluorescence spectra of single crystals clearly showed an excimerlike delocalized excited state owing to the short distance between neighboring [7]carbohelicene units.

Introduction

Helical chirality is ubiquitous in biological molecular systems such as DNA, proteins, and nucleic acids.[1] In general, helix formation seems to be a quasi-universal option for high-order spatial organization of matter at both microscopic and macroscopic levels. Such a prominent role of one-dimensional helical arrangements in natural systems has recently stimulated the curiosity of researchers in the fields of materials chemistry and related photochemistry, for example, chiral recognition,[2] separation,[3] switching,[4] and optoelectronics.[5]

To construct designed helical molecular superstructures, synthetic strategies such as covalent and noncovalent self-assembled organization of various chiral and achiral units have been commonly utilized. Macromolecular organization exclusively through covalent bonding is uncommon because of the synthetic difficulty and poor solubility.[6] Representative examples are helical polyacetylenes with continuous π conjugation through covalent bonds.[7] In contrast, supramolecular methods utilizing intermolecular interactions such as π–π interactions,[5a,8] van der Waals interactions,[5e,9] hydrogen bonds,[3b,4e,10] and coordination bonds[4c,8e,11] are powerful tools. Supramolecular techniques make it possible to achieve novel phenomena including spectroscopic and optical properties in comparison with those of the corresponding monomeric forms.[12] On the one hand, π–π interactions in organized structures are especially known to yield new emissive states, such as excimers.[13] On the other hand, excimer formation also reveals details of the superstructure. Accordingly, appropriate organization by both covalent and noncovalent bonding/interaction is essential for construction of one-dimensional macromolecular helical systems.

To obtain the above photofunctionalized and helical macromolecular systems, carbohelicene is a good candidate as the

---

[a] Dr. H. Sakai, S. Shinto, Prof. T. Hasobe
Department of Chemistry, Faculty of Science and Technology
Keio University, Yokohama, Kanagawa 223-8522 (Japan)
Fax: (+81) 45-566-1697
E-mail: hasobe@chem.keio.ac.jp

[b] Prof. Y. Araki, Prof. T. Wada
Institute of Multidisciplinary Research for Advanced Materials
Tohoku University, 2-1-1 Katahira, Aoba-ku, Sendai 980-8577 (Japan)
Fax: (+81) 22-217-5608
E-mail: araki@tagen.tohoku.ac.jp

[c] Prof. T. Sakanoue, Prof. T. Takenobu
Department of Applied Physics, Waseda University
3-4-1, Okubo, Shinjuku, Tokyo 169-8555 (Japan)
Fax: (+81) 3-5286-2981
E-mail: takenobu@waseda.jp

Supporting information for this article is available on the WWW under http://dx.doi.org/10.1002/chem.201402426.

basic molecular unit. Carbohelicenes are polycyclic aromatic hydrocarbons composed of *ortho*-condensed benzene rings. The steric hindrance arising in this *ortho* condensation precludes planarity for molecules with sequences of five or more rings and causes the π-conjugated structures to become distorted into helices with intrinsically chiral structures.[14] Consequently, carbohelicenes exhibit unique optical properties, for example, high anisotropy factor ($g = \Delta\varepsilon/\varepsilon$) with increasing the number of *ortho*-condensed benzene units.[15] Sapir and co-workers reported the detail excited-state dynamics of carbohelicenes. In the range of 5–9 benzene units (i.e., [5]- to [9]carbohelicene), the fluorescence quantum yields Φ_{FL} are approximately zero, whereas the quantum yields of intersystem crossing Φ_{ISC} exceed 0.9.[16] Thus far, the number of publications concerning the excited-state dynamics of carbohelicenes is limited, so new synthetic strategies to control the excited-state dynamics are essential for high fluorescence quantum yields and subsequent further development of optical applications such as circularly polarized luminescence.[17]

According to the previous reports and a database of single-crystal structures of helicenes, one-dimensional columnar helical packing driven by π–π stacking interactions is unusual, and the major structural motif of helicenes is noncolumnar packing driven by CH⋯π interactions.[1c,18] Recently, Nozaki and co-workers reported one-dimensional column formation of chiral λ^5-phospha[7]helicenes by utilizing dipole–dipole interaction in addition to π–π stacking interactions.[19] Similar one-dimensional helix formation by heterochiral crystals has been already reported.[20] However, one-dimensional columnar helical structures of racemic helicene derivatives in the single-crystal state have yet to be reported, although there are a few reports concerning the corresponding one-dimensional nonhelical structures.[20c,21]

Quinoxalines (i.e., benzopyrazines) have a synthetic advantage over other aromatic compounds because of their convenient synthesis from diketones and diamines.[22] Quinoxalines show strongly electron-accepting behavior due to their high electron affinity, which is derived from the two unsaturated nitrogen atoms. Accordingly, benzopyrazines are widely utilized as light-emitting and electron-transporting materials because of the highly polarized nature of the imine units in the pyrazine ring.[22] Additionally, the polarized nature of a quinoxaline unit may have an effect on the crystal packing. Various small organic molecules, including promising p-type organic materials such as oligoacences, show a herringbone packing motif. However, if the benzene rings are replaced by pyrazine rings, the crystal stacking motif originating from CH⋯π interactions changes to intracolumn π stacking between two neighboring molecules and intercolumn CH⋯N interactions between two neighboring columns.[23]

In view of the above points, we synthesized a series of quinoxaline-fused [7]carbohelicene derivatives (Figure 1). The integration of quinoxaline and [7]carbohelicene units contributes to the control of spectroscopic behavior (e.g., fluorescence) in the monomeric form and the structural properties in the aggregate state. In particular, formation of one-dimensional helical columns by a racemic bis(4-methoxyphenyl)-substituted quinoxaline-fused [7]carbohelicene in the single crystal is noteworthy. The helical columnar structure is mainly formed by intracolumn π–π stacking interaction between two neighboring carbohelicene units and intercolumn CH⋯N interaction between a nitrogen atom in a quinoxaline unit and a hydrogen atom in a helicene unit, which is in sharp contrast to the packing motif of the corresponding enantiomer. Moreover, the excimerlike delocalized excited state originating from neighboring carbohelicene units in the single crystal was clearly observed by time-resolved fluorescence measurements.

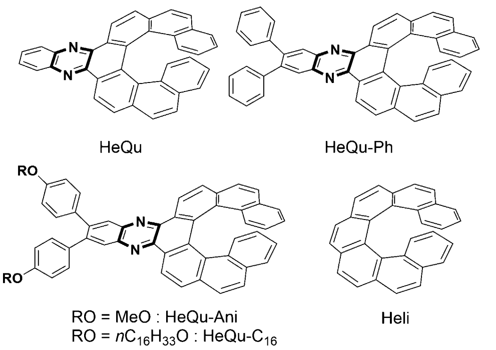

Figure 1. Chemical structures of quinoxaline-fused [7]carbohelicenes in this study.

Results and Discussion

Synthesis

As mentioned above, quinoxalines can be simply synthesized from diketones. We used this synthetic strategy to synthesize a series of quinoxaline-fused [7]carbohelicene derivatives. [7]Carbohelicene 1,2-diketone (He-Ket) was obtained from 1,2-dimethoxy [7]carbohelicene (He-OMe; Scheme 1). First, He-OMe was synthesized by the reported synthetic method of Harrowven and co-workers.[24] Next, He-Ket was obtained by dihydroxylation of He-OMe, which was followed by dehydration. The yield of the above two steps was 64%. Finally, quinoxaline-fused [7]carbohelicenes were synthesized by dehydration of He-Ket and corresponding 1,2-diaminobenzene derivatives under appropriate synthetic conditions (Table 1).

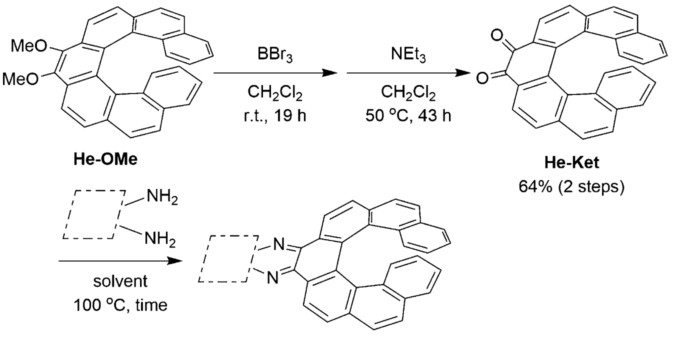

Scheme 1. Synthesis of quinoxaline-fused [7]carbohelicenes.

Table 1. Synthetic conditions and yields of new quinoxaline-fused [7]carbohelicenes.

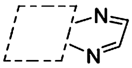	Solvent	T [h]	Yield [%]
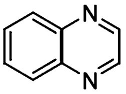 HeQu	AcOH	1	65
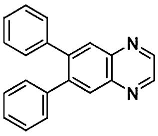 HeQu-Ph	AcOH/CHCl$_3$ (1/5 v/v)	3	68
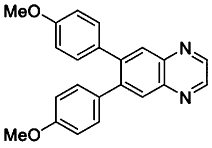 HeQu-Ani	AcOH/EtOH (1/2 v/v)	3	62
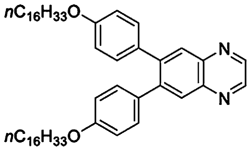 HeQu-C$_{16}$	AcOH/EtOH/CH$_2$Cl$_2$ (1/1/1 v/v/v)	1	63

Electrochemical properties of quinoxaline-fused [7]carbohelicenes

The electrochemical properties of quinoxaline-fused [7]carbohelicenes were investigated by using cyclic voltammetry (CV) and differential pulse voltammetry (DPV) to examine the substituent effects on the reduction and oxidation potentials. A typical voltammogram of HeQu-Ani in CH$_2$Cl$_2$ containing 0.1 M nBu$_4$NPF$_6$ is shown in Figure 2. Supporting Information Figure S1 shows cyclic and differential pulse voltammograms of HeQu and HeQu-Ph, respectively. The electrochemical potentials of quinoxaline-fused [7]carbohelicenes and reference Heli are summarized in Table 2. Two reversible redox couples, corresponding to the first and second reduction processes of HeQu derivatives, were observed, whereas one quasireversible oxidation peak was found in all of the cyclic voltammograms for HeQu derivatives. The first reduction (E_{red1}) and oxidation (E_{ox}) potentials of HeQu-Ani in CH$_2$Cl$_2$ were determined to be −1.31 V and 1.43 V versus SCE, respectively. These redox potentials are quite similar to those of HeQu ($E_{\mathrm{red1}}=-1.34$, $E_{\mathrm{ox}}=1.47$ V) and HeQu-Ph ($E_{\mathrm{red1}}=-1.28$, $E_{\mathrm{ox}}=1.47$ V). Compared to the reported first reduction ($E_{\mathrm{red1}}=-2.02$ V) and oxidation ($E_{\mathrm{ox}}=1.42$ V) potentials of reference compound Heli, the first oxidation potentials of HeQu derivatives are similar to that of Heli, whereas the corresponding first reduction potential is significantly shifted to positive direction by about 0.7 V.

The HOMO and LUMO levels calculated by the DFT method at the B3LYP/6-31G* level of theory also support the above trends observed in electrochemical data (Figure 3, Supporting

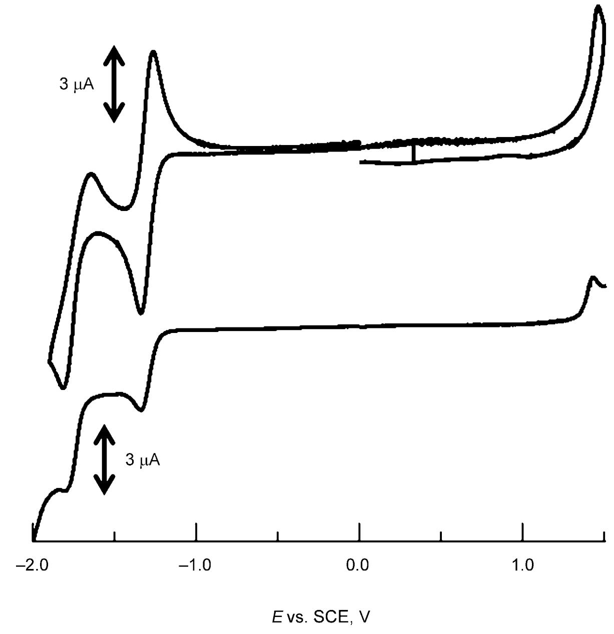

Figure 2. Cyclic and differential pulse voltammograms of HeQu-Ani in CH$_2$Cl$_2$ with 0.1 M nBu$_4$NPF$_6$ as supporting electrolyte. Scan rate: 0.05 V s^{-1} for CV and 0.01 V s^{-1} for DPV.

Table 2. Electrochemical properties and energy levels of HeQu derivatives and Heli.

Helicene	E_{ox}[a,b] [V]	E_{red1}[a]	E_{red2}[a] [V]	E_{HOMO}[c] [eV]	E_{LUMO}[c] [eV]
HeQu	1.47 (−5.74 eV)[d]	−1.34	−1.78	−5.47	−2.26
HeQu-Ph	1.47 (−5.74 eV)[d]	−1.28	−1.72	−5.44	−2.29
HeQu-Ani	1.43 (−5.70 eV)[d]	−1.31	−1.73	−5.37	−2.19
Heli	1.42[e] (−5.69 eV)[d]	−2.02[e]		−5.36	−1.49

[a] Volts vs. SCE. [b] Determined by DPV. [c] Calculated by DFT at the B3LYP/6-31G* level of theory. [d] Calculated HOMO levels (E_{HOMO}) from the following equation: $E_{\mathrm{HOMO}}=E_{1/2}(\mathrm{Fe/Fe^+})+4.80$.[25] [e] Reported value in MeCN.[26]

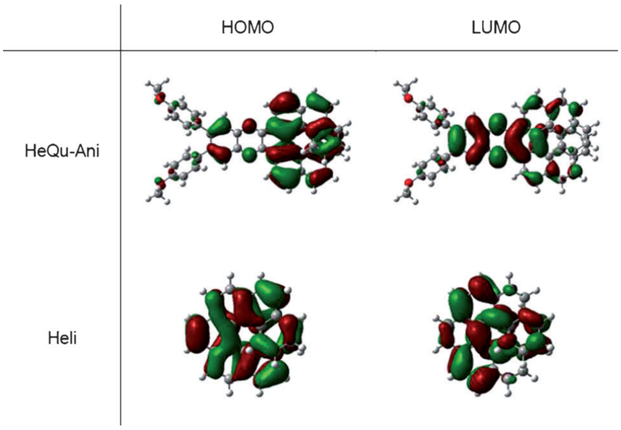

Figure 3. Molecular orbitals of HeQu-Ani and Heli (B3LYP/6-31G* level of theory).

Information Figure S2, and Table 2). The experimental results are comparable to those determined by DFT calculations (Table 2). The HOMO and LUMO are localized on helicene and quinoxaline units, respectively (Figure 3). This trend is totally different from the molecular orbitals of Heli. In contrast to the similar HOMO levels of HeQu derivatives and Heli, the LUMO levels of HeQu derivatives are strongly stabilized as compared to that of Heli. The decrease in HOMO–LUMO gap may have an effect on the spectroscopic properties (see below).

Steady-state absorption spectra of quinoxaline-fused [7]carbohelicene derivatives

The steady-state spectroscopic properties of the quinoxaline-fused [7]carbohelicenes was studied by means of absorption, circular dichroism (CD), and fluorescence measurements. Figure 4 shows absorption spectra of HeQu derivatives. The spectra of HeQu (Figure 4a) and HeQu-Ani (Figure 4b) are significantly redshifted and broadened compared to the corresponding Heli reference system (Figure 4c). The spectrum of HeQu-Ph is nearly identical to that of HeQu-Ani (Supporting Information Figure S3). Considering the above electrochemical data and DFT calculations (Table 2), a plausible reason for the redshifts is lowering of the LUMO relative to the HOMO levels on introducing an electron-withdrawing quinoxaline unit, which leads to a decrease in the HOMO–LUMO gap. Moreover, we also calculated the molar extinction coefficients ε_{0-0} from the 0–0 absorption bands (Table 4). The absorption peak of Heli $\varepsilon_{0-0} = 474\,\mathrm{M^{-1}\,cm^{-1}}$) at 410 nm was originally assigned to a symmetry forbidden transition.[27] However, these transitions become allowed when the symmetry is reduced. Therefore, the ε_{0-0} values of HeQu derivatives increase strongly with increasing bulkiness of the substituents.

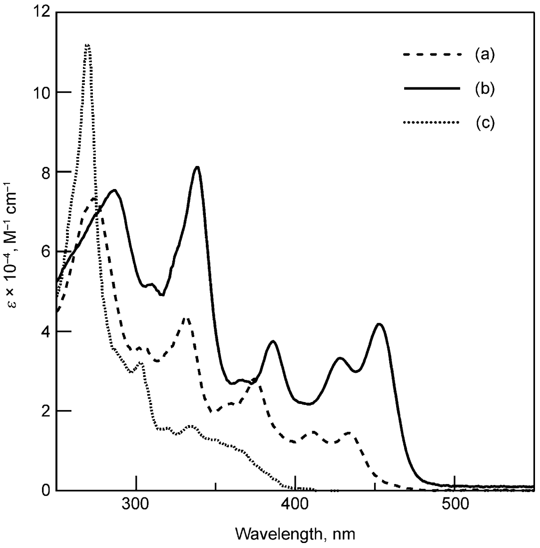

Figure 4. UV/Vis spectra of a) 2.0 μM HeQu in THF, b) 2.0 μM HeQu-Ani in THF, and c) Heli in CH_2Cl_2. Spectrum c was reproduced from ref. [27].

CD spectra of quinoxaline-fused [7]carbohelicene derivatives

The separation of enantiomers from racemic mixtures was accomplished by HPLC on a chiral column. Then, we measured CD spectra of HeQu derivatives to assign the helicity (Figure 5 and Supporting Information Figure S4). In all cases, they demonstrate mirror-image values of the (+) and (−) enantiomers within the experimental error. A decreasing trend in $\Delta\varepsilon$ values of HeQu derivatives was observed over the wavelength range of 250–300 nm compared to Heli, whereas the $\Delta\varepsilon$ value increased in the range of 400–500 nm. Thus, attachment of quinoxaline to helicene units induced chirality in both UV and visible regions because of the expanded π-conjugation. We also explored in greater detail the relations among the molecular absorption coefficients ε and anisotropy factors g_{CD} of these molecules at absorption maximum wavelength (Table 3). For example, ε and $\Delta\varepsilon$ of Heli at 351 nm are $11\,800\,\mathrm{M^{-1}\,cm^{-1}}$ and $263\,\mathrm{M^{-1}\,cm^{-1}}$, respectively. Thus, g_{CD} was estimated to be 22.3×10^{-3}.[15b] The date of the HeQu derivatives are summarized in Table 3.

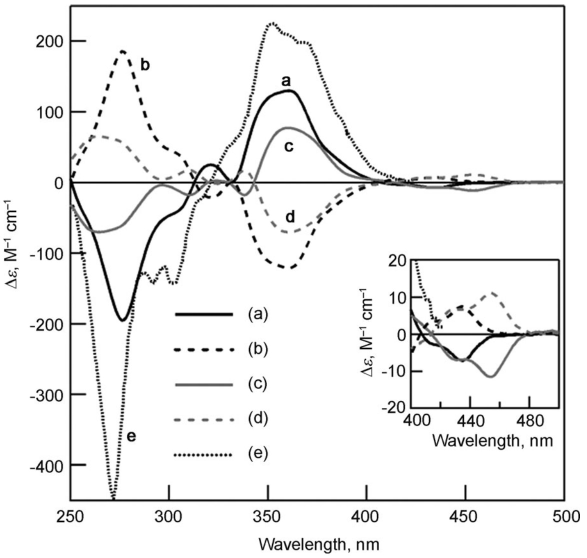

Figure 5. CD spectra of a) *P*-HeQu in THF, b) *M*-HeQu in THF, c) *P*-HeQu-Ani in THF, d) *M*-HeQu-Ani in THF, and e) *P*-Heli in $CHCl_3$. Spectrum e was reproduced from ref. [15b].

Table 3. Optical properties of HeQu derivatives and Heli.

Helicene	λ_{obs} [nm]	E [$\mathrm{M^{-1}\,cm^{-1}}$]	$\Delta\varepsilon$ [$\mathrm{M^{-1}\,cm^{-1}}$]	g_{CD}
HeQu	351	20 200	121	6.21×10^{-3}
HeQu-Ph	357	21 200	103	4.85×10^{-3}
HeQu-Ani	360	26 900	77.5	2.88×10^{-3}
Heli[a]	351	11 800	263	22.3×10^{-3}

[a] Reported value in $CHCl_3$.[15b]

Steady-state fluorescence spectra of quinoxaline-fused [7]carbohelicene derivatives

Fluorescence spectra of HeQu derivatives were measured in THF at an excitation wavelength of 330 nm (Figure 6 and Supporting Information Figure S5). The fluorescence spectra of HeQu (Figure 6a) and HeQu-Ani (Figure 6b) are similar and they are significantly redshifted by about 70 nm relative to that of reference Heli (Figure 6c). This trend is also similar to that in absorption measurements, and is attributable to the decrease in HOMO–LUMO gap because of the lowered of LUMO levels.

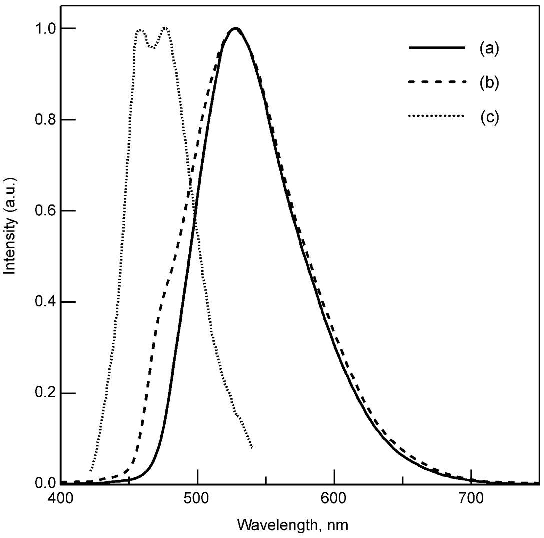

Figure 6. Fluorescence spectra of a) 2.0 μм HeQu in THF, $\lambda_{ex}=330$ nm, b) 2.0 μм HeQu-Ani in THF, $\lambda_{ex}=330$ nm, and c) Heli in 1,4-dioxane. Spectrum c was reproduced from ref. [28].

Quantum yields and fluorescence lifetimes of quinoxaline-fused [7]carbohelicene derivatives in solution

To evaluate the light-emitting properties of HeQu derivatives, first we determined their absolute fluorescence quantum yields Φ_{FL} (Table 4). The Φ_{FL} values of HeQu (0.07), HeQu-Ph (0.05), and HeQu-Ani (0.05) are larger than that of Heli (0.02). In particular, the Φ_{FL} value of HeQu is about four times larger than that of Heli. Although the Φ_{FL} values of HeQu derivatives bearing aryl groups decrease slightly compared to that of pristine HeQu, introduction of quinoxaline units enhanced the Φ_{FL} values slightly compared to Heli.

Table 4. Spectroscopic properties of HeQu derivatives and Heli.[a]

Helicene	Φ_{FL}[c]	τ_{FL}[d] [ns]	$k_{FL}\times10^{6}$ [s^{-1}]	$k_{other}\times10^{7}$ [s^{-1}]	ε_{0-0} [$M^{-1}cm^{-1}$]
HeQu	0.07	2.70	25.6	34.5	14500 (434 nm)
HeQu-Ph	0.05	2.46	19.5	38.7	25000 (447 nm)
HeQu-Ani	0.05	2.05	23.4	46.4	41800 (452 nm)
Heli[b]	0.02	13.8	1.52	7.09	474 (410 nm)

[a] Φ_{FL}: fluorescence emission quantum yield measured in 2.0 μм THF solution, τ_{FL}: fluorescence lifetime, k_{FL}: fluorescence emission rate constant, k_{other}: total rate constant of other pathways, ε_{0-0}: molar extinction coefficient of 0-0 absorption band. $\Phi_{FL}=k_{FL}\ \tau_{FL}=k_{FL}/(k_{FL}+k_{other})$. [b] Reported value in 1,4-dioxane.[13e,28,29] [c] Excited at 330 nm. [d] Excited at 390 nm.

To further investigate the light-emitting properties of HeQu derivatives, fluorescence lifetime measurements were performed. The fluorescence decays of HeQu derivatives were examined in THF solution with pulsed 390 nm laser light (Figure 7). The fluorescence lifetimes τ_{FL}, which were evaluated from monoexponential fittings, are summarized in Table 4. τ_{FL} values of HeQu (2.70 ns), HeQu-Ph (2.46 ns), and HeQu-Ani (2.05 ns) are much shorter than that of Heli (13.8 ns).[13e,18a,b] To discuss the excited-state dynamics in detail, the net rate constants of fluorescence emission k_{FL} and other processes k_{other} were determined (Table 4). The k_{FL} values of HeQu derivatives are one order of magnitude greater than that of Heli. This is in sharp contrast to small increases of k_{other} values in HeQu derivatives relative to Heli. It is well-known that k_{FL} is significantly related to the molar extinction coefficient for absorption.[30] Therefore, we estimated the molar extinction coefficients of 0–0 absorption bands ε_{0-0} (Table 4). HeQu derivatives have large ε_{0-0} values relative to that of Heli. The increasing trend in ε_{0-0} values agrees well with that in k_{FL}. On the basis of these results, we can conclude that introduction of quinoxaline units successfully contributes to improved light-emitting properties of HeQu derivatives.

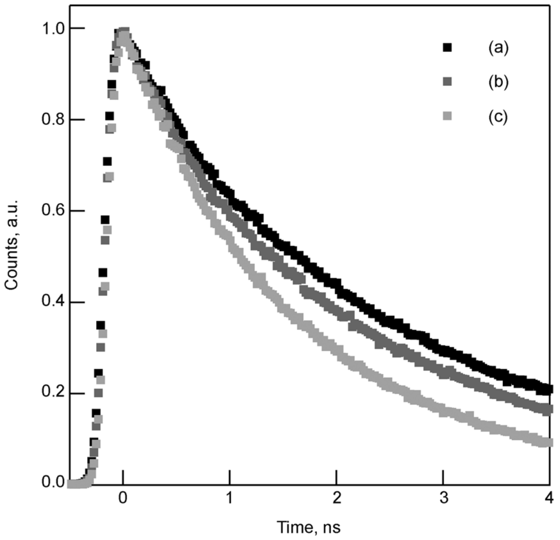

Figure 7. Typical fluorescence decays of a) 2.0 μм HeQu in THF, b) 2.0 μм HeQu-Ph in THF, and c) 2.0 μм HeQu-Ani in THF. The excitation wavelength was 390 nm.

Analyses of single-crystal structures

Single-crystal structures were determined by X-ray analysis to evaluate the aggregate properties of HeQu derivatives. We prepared single crystals of HeQu derivatives for X-ray diffraction analysis by vapor diffusion at room temperature (see Experimental Section), and the crystal data are summarized in Supporting Information Table S1. Reference compound *rac*-Heli

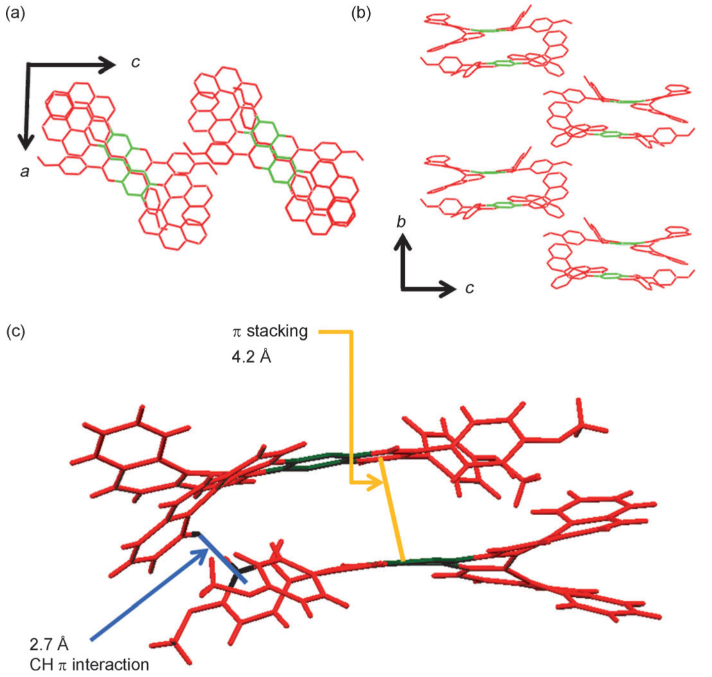

Figure 8. Single-crystal structures of *P*-HeQu-Ani. Red: *P* enantiomer, green: pyrazine ring. a) Packing mode along the *b* axis. Hydrogen atoms have been omitted for clarity. b) Packing mode along the *a* axis. Hydrogen atoms have been omitted for clarity. c) π-stacking between two neighboring *P*-HeQu-Ani with intermolecular distance. Yellow line: π-stacking distance d_p. Blue line: CH⋅⋅⋅π interaction distance.

shows a nonhelical crystal structure based on CH⋅⋅⋅π interactions (see Supporting Information Figure S6). The crystal structures of *P*-HeQu-Ani and *rac*-HeQu-Ani are depicted in Figures 8 and 9, respectively. *P*-HeQu-Ani forms dimers by virtue of π-stacking between two neighboring quinoxaline units and CH⋅⋅⋅π interactions between helicene units (Figure 8a and b). As discussed above,[23] quinoxalines form intracolumn π-stacked structures in the aggregate state. The π-stacking distance d_p was estimated to be 4.2 Å (yellow line in Figure 8c). The distance of the CH⋅⋅⋅π interaction between 4-methoxyphenyl group and helicene was calculated to be 2.7 Å (blue line in Figure 8c).

In contrast to *P*-HeQu-Ani, *rac*-HeQu-Ani exhibits one-dimensional and helical column formation along the crystallographic *c* axis by virtue of intracolumn interaction between nearest two helicene units (Figure 9a and b). In the intracolumn direction, face-to-face and π–π interactions of helicene units occur (Figure 9c). The *P*-HeQu-Ani and *M*-HeQu-Ani conformers are alternately stacked in the same column. The π-stacking distance d_p was estimated to be 3.6 Å (yellow line in Figure 9c). In addition, intercolumn CH⋅⋅⋅N interactions between nitrogen atoms in quinoxaline units and hydrogen atoms in helicene units was observed. The CH⋅⋅⋅N distance is 3.4 Å (black line in Figure 9b). This is in sharp contrast to the formation of π-stacked dimers of quinoxaline units in *P*-HeQu-Ani. Thus, utilization of racemic HeQu-Ani successfully induced intracolumn π stacking between two helicene units in *P*- and *M*-HeQu-Ani and intercolumn CH⋅⋅⋅N interaction between two neighboring columns to form one-dimensional columnar structures.

To investigate the substituent effect (i.e., 4-methoxyphenyl group) on one-dimensional column formation, we also compared the crystal structures of *rac*-HeQu-Ph and *rac*-HeQu-Ani (Figure 9 and Supporting Information Figure S7). In contrast to *rac*-HeQu-Ani, *rac*-HeQu-Ph shows dimer formation by virtue of π stacking between two neighboring quinoxaline units and

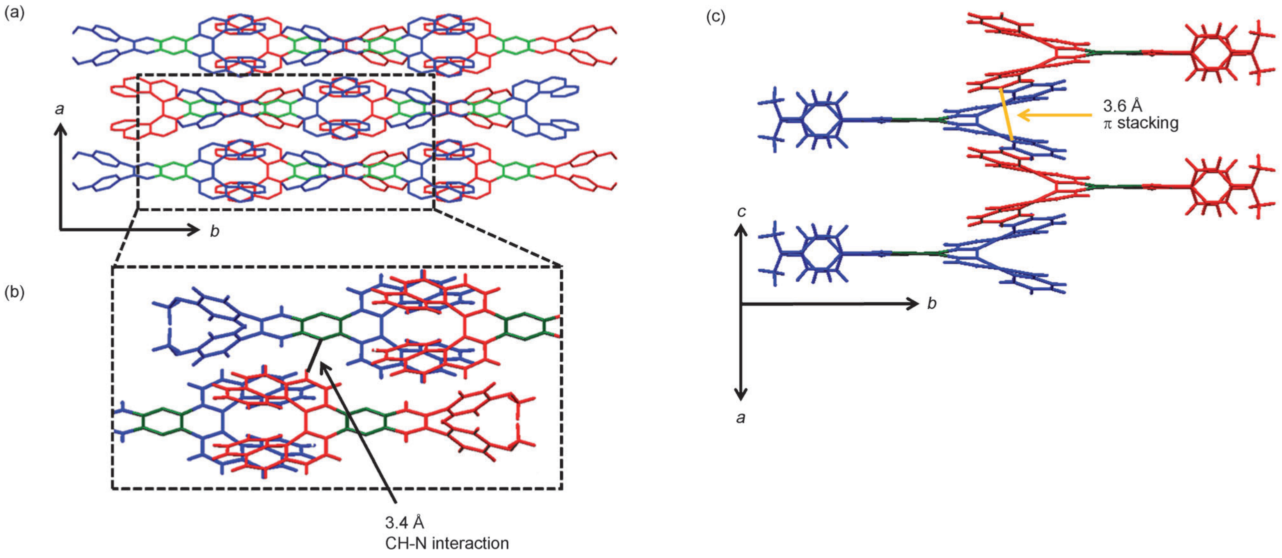

Figure 9. Single-crystal structures of *rac*-HeQu-Ani. Red: *P* enantiomer, blue: *M* enantiomer, green: pyrazine ring. a) Packing mode along *c* axis. Hydrogen atoms have been omitted for clarity. b) A view of the neighboring columns showing intermolecular distances. Black line: CH⋅⋅⋅N interaction distance. c) Helical columnar structure of *rac*-HeQu-Ani with intermolecular π-stacking distance d_p.

CH···π interaction between helicene units of *P*- and *M*-HeQu-Ph (Supporting Information Figure S7 a and b). This comparison indicates that the relatively bulky 4-methoxyphenyl group hampered π–π interactions between quinoxaline units and induced the above-mentioned one-dimensional column formation (Figure 9).

To further check the substituent effects on the aggregate properties, the crystal structure of *rac*-HeQu was also determined (Supporting Information Figure S8). As a consequence, in this case, we could not find one-way column formation of racemic helicenes. A plausible reason is the occurrence of molecular packing formations based on CH···π interactions. In particular, in the case of *rac*-HeQu, the crystal structure shows conglomerates based on CH···π interactions. Moreover, in the case of *rac*-HeQu-C_{16} with long alkyl chains, typically dozens of nanosized fibrous structures (see the TEM image in Supporting Information Figure S9) were obtained by a simple drop-casting method using methylcyclohexane. Therefore, we can conclude that introduction of relatively bulky 4-methoxyphenyl-linked quinoxaline onto [7]carbohelicene unit induced one-dimensional and helical column formation in the racemic single crystal.

Time-resolved fluorescence spectra of HeQu derivatives in single crystal states

To evaluate the intermolecular interactions in the excited states, time-resolved fluorescence spectra and the corresponding decay-time profiles were measured (Figure 10). Figure 10 a and c show time-resolved spectra of *rac*-HeQu and *P*-HeQu-Ani single crystals. To clarify the spectral shapes, the fluorescence intensities of these spectra were equally normalized. On laser-pulse excitation at 390 nm, we first observed a broad fluorescence spectrum with a maximum peak at around 550 nm. This is probably attributable to the monomeric HeQu derivatives by comparison with the steady-state fluorescence spectrum in THF solution (Figure 6 a and b). This band monotonously decreases with increasing time. In contrast, we found a new band with a peak maximum around 590 nm in addition to the above monotonous decrease of fluorescence intensity at 550 nm for single-crystal *rac*-HeQu-Ani. The new band may be ascribed to the excimerlike delocalized excited state (Figure 10 e).

To further discuss the excited-state dynamics, we analyzed decay lifetimes in two different wavelength regions: 510–530 nm and 600–650 nm (Figure 10 b, d, and f). The decay curves of the fluorescence intensity could be fitted as double

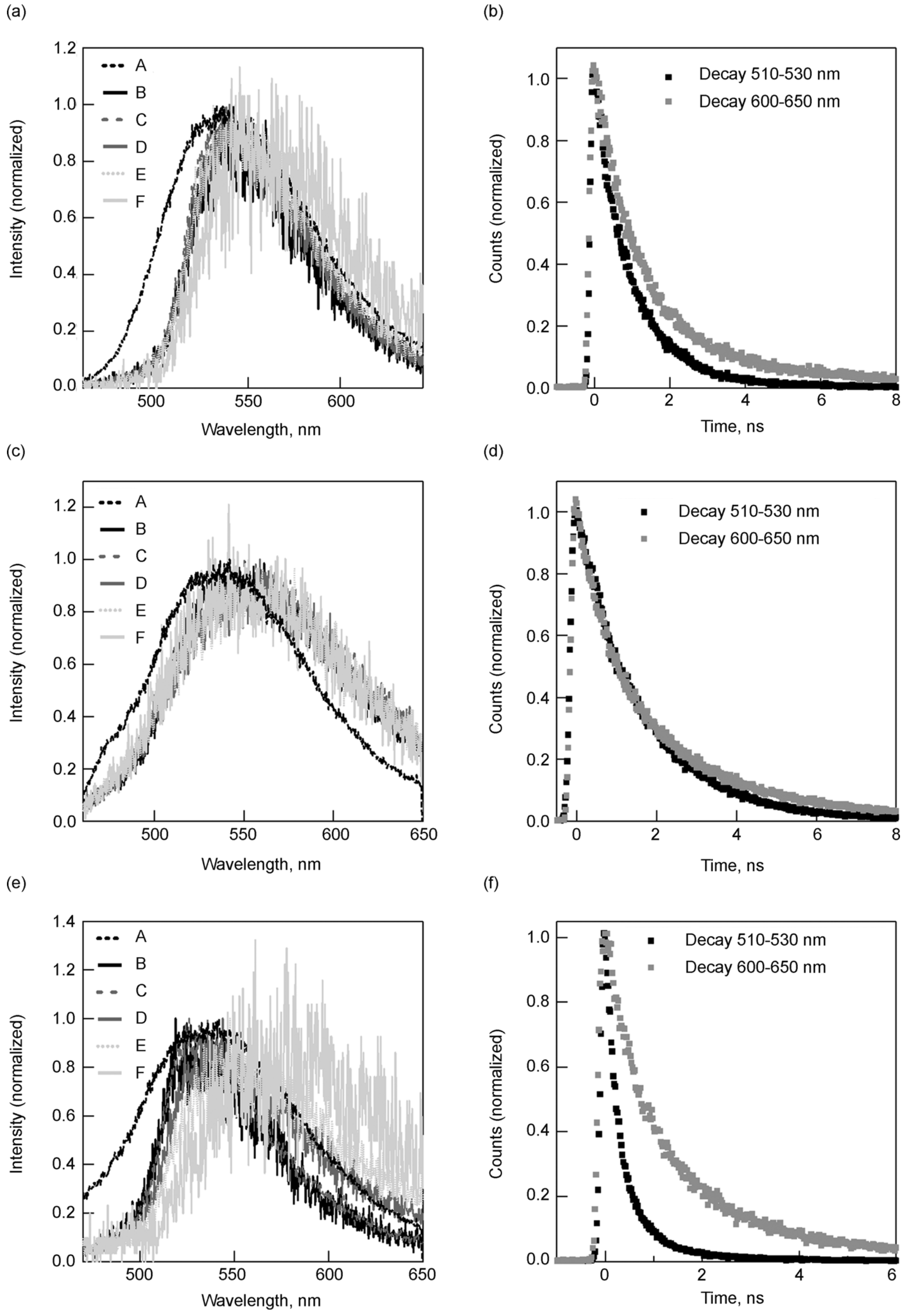

Figure 10. Time-resolved fluorescence spectra and fluorescence lifetime decays of single crystals. a) spectra of *rac*-HeQu, b) decays of *rac*-HeQu, c) spectra of *P*-HeQu-Ani, d) decays of *P*-HeQu-Ani, e) spectra of *rac*-HeQu-Ani, and f) decays of *rac*-HeQu-Ani. The excitation wavelength was 390 nm. A: monomer for comparison, B: 1.00 ns, C: 1.50 ns, D: 2.00 ns, E : 2.50 ns, and F: 3.00 ns.

Table 5. Fluorescence lifetimes of assemblies of HeQu derivative.

Helicene	τ_{FL} [ns], 510–530 nm	τ_{FL} [ns], 600–650 nm
rac-HeQu-Ani	0.30 (89.8%) 1.14 (10.2%)	0.84 (79.4%) 2.97 (20.6%)
P-HeQu-Ani	0.73 (21.9%) 1.83 (78.1%)	0.86 (55.0%) 2.90 (45.0%)
rac-HeQu	0.88 (90.0%) 1.96 (10.0%)	1.05 (82.8%) 4.21 (17.2%)

exponentials, and the fluorescence lifetimes are listed in Table 5. In the 510–530 nm region, the τ_{FL} value of *rac*-HeQu-Ani crystal (0.30 ns) is much shorter than those of *P*-HeQu-Ani (0.73 ns) and *rac*-HeQu (0.88 ns) crystals. A plausible mechanism of the strong quenching process may be singlet–singlet annihilation of helicene units. As discussed above, in *rac*-HeQu-Ani crystals, adjacent face-to-face and π–π interaction of helicene units was observed, for which the d_p value of 3.6 Å is smaller than that of 4.2 Å in *P*-HeQu-Ani (Figures 8c and 9c). Furthermore, the molecular packing formation of *rac*-HeQu is based on CH⋅⋅⋅π interactions. Hence, in the case of *rac*-HeQu-Ani, singlet–singlet annihilation and the subsequent excimer-like delocalized excited state continuously occur in the *rac*-HeQu-Ani crystal. Thus, we have successfully observed a peculiar photophysical process in the one-dimensional helical columnar structure.

Conclusion

We designed and synthesized a series of quinoxaline-fused [7]carbohelicenes. The electrochemical and spectroscopic properties of these compounds were evaluated by electrochemical methods, steady-state and time-resolved spectroscopy, and DFT calculations. In contrast to the similar first oxidation potentials of HeQu derivatives and Heli, the first reduction potentials of HeQu derivatives were shifted to the positive ($\approx$0.7 V) by introducing quinoxaline units. The steady-state absorption, fluorescence, and CD spectra became redshifted compared to the reference Heli. These trends were explained by the HOMO and LUMO levels and molecular orbitals calculated by DFT methods. We further investigated the absolute fluorescence quantum yields Φ_{FL} of HeQu derivatives. The maximum Φ_{FL} of HeQu derivatives is about four times larger than that of reference Heli. The enhancement of Φ_{FL} is plausibly attributable to relative acceleration of the net rate constant of fluorescence emission k_{FL}.

In the single-crystal structures, by introducing appropriate substituents (i.e., 4-methoxyphenyl groups) onto the HeQu unit, one-dimensional helical column formation, which is based on intracolumn π stacking between two [7]carbohelicene units and intercolumn CH⋅⋅⋅N interactions between two neighboring columns, was successfully observed in the racemic single-crystal state. This is in sharp contrast to formation of π-stacked dimers of quinoxaline units by *P*-HeQu-Ani. Moreover, in the time-resolved fluorescence measurements, an excimerlike delocalized excited state between neighboring [7]carbohelicene units was observed because of the short distance between two helicene units. Such synthetic and supramolecular strategies for helicene derivatives will provide a new perspective for future development of optoelectronic applications.

Experimental Section

General and materials

All solvents and reagents of the best grade available were purchased from commercial suppliers such as Tokyo Chemical Industry, Kanto Chemical Co., Inc., Nacalai Tesque, Wako Pure Chemical Industries, and Sigma-Aldrich. All commercial reagents were used without further purification. Column flash chromatography was performed on silica gel (Kanto Chemical Silica Gel 60N, 40–50 μm or 100–210 μm). Preparative recycling gel-permeation chromatography was performed with an HPLC apparatus (Japan Analytical Industry LC-9204) by using chloroform as eluent at room temperature. This system is equipped with a pump (JAI PI-60, flow rate 3.5 mL min^{-1}), a UV detector (JAI UV-3740), and two columns (JAIGEL-2H and JAIGEL-1H, both 40×600 mm). Racemic [7]carbohelicene derivatives were separated by using hexane/chloroform (2/1, v/v) as eluent at room temperature on a DAICEL CHIRALPAK IA column. ^{1}H NMR and ^{13}C NMR spectra were acquired on a JEOL ECX-400, AL-400, or ALPHA-400 spectrometer by using the solvent peak as the reference standard, with chemical shifts given in parts per million (ppm). $CDCl_3$ was used as NMR solvent. The ^{1}H NMR and ^{13}C NMR spectra are shown in Supporting Information Figure S10–S31. MALDI-TOF mass spectra were recorded on a Bruker Ultraflex instrument. The DFT calculations of molecular orbitals were performed with Gaussian 03 at the B3LYP/6-31G* level of theory. The molecular geometries were optimized at the same level.[31]

Syntheses

He-Ket: 6.80 mL of BBr_3 solution (ca. 1.0 M in CH_2Cl_2) was added dropwise over 10 min to a solution of He-OMe (113 mg, 0.26 mmol) in dry CH_2Cl_2 (150 mL) on an ice bath. The resulting solution was stirred at room temperature for 19 h under nitrogen atmosphere. The reaction mixture was quenched with water. Then, the product was extracted with CH_2Cl_2, washed with brine, and dried over anhydrous Na_2SO_4. After solvent evaporation, the crude product as a black solid (190 mg) was dissolved in CH_2Cl_2 (55 mL) and NEt_3 (2.0 mL, 14.4 mmol). Next, the solution was stirred at 50 °C for 43 h. After cooling, the solution was poured onto water, and then the organic layer was extracted with CH_2Cl_2, washed with brine, dried over anhydrous Na_2SO_4, and evaporated. Finally, flash column chromatography on silica gel with hexane/ethyl acetate (10/1 v/v) as eluent afforded He-Ket as a red solid (67.6 mg, 0.17 mmol, 64%). ^{1}H NMR (400 MHz, $CDCl_3$): $\delta = 8.31$ (d, $J = 8.1$ Hz, 2H), 7.89 (d, $J = 8.1$ Hz, 2H), 7.54 (d, $J = 8.8$ Hz, 2H), 7.47 (d, $J = 8.8$ Hz, 2H), 7.26–7.24 (m, 2H), 6.99 (dd, $J = 7.4$, 3.7 Hz, 2H), 6.64 (d, $J = 8.3$ Hz, 2H), 6.41 ppm (dd, $J = 7.6$, 3.8 Hz, 2H); ^{13}C NMR (100 MHz, $CDCl_3$): $\delta = 182.5$, 139.2, 137.9, 132.0, 131.0, 130.6, 129.4, 129.2, 127.7, 127.1, 126.5, 125.8, 125.6, 125.2, 124.0; MALDI-TOF MS: $m/z = 409$ $[M+H]^{+}$ (Supporting Information Figures S18 and S19).

HeQu: He-Ket (30.1 mg, 0.074 mmol) and *o*-phenylenediamine (9.68 mg, 0.09 mmol) were dissolved in acetic acid (6.5 mL) and the mixture stirred at 100 °C for 1 h. After neutralization with dilute aqueous NaOH solution, the organic phase was extracted with CH_2Cl_2, washed with brine, and dried over Na_2SO_4, and the solvent was evaporated. The product was purified by silica gel column chromatography with hexane/ethyl acetate (1/1 v/v) as eluent to afford HeQu as a yellow solid (22.9 mg, 0.073 mmol, 65 %). ^{1}H NMR (400 MHz, $CDCl_3$): $\delta = 9.56$ (d, $J = 7.8$ Hz, 2 H), 8.45 (dd, $J = 6.3$, 3.4 Hz, 2 H), 8.16 (d, $J = 8.3$ Hz, 2 H), 7.92 (dd, $J = 6.8$, 3.4 Hz, 2 H), 7.74 (d, $J = 8.8$ Hz, 2 H), 7.50 (d, $J = 8.3$ Hz, 2 H), 7.30 (d, $J = 7.3$ Hz, 2 H), 6.99–6.96 (m, 4 H), 6.45 ppm (dd, $J = 7.1$, 3.5 Hz, 2 H); ^{13}C NMR (100 MHz, $CDCl_3$): $\delta = 142.9$, 142.3, 133.5, 131.7, 129.7, 129.5, 129.4, 129.2, 128.5, 128.4, 128.2, 126.6, 125.6, 125.4, 124.9, 123.7, 122.8 ppm; MALDI-TOF MS: $m/z = 480$ $[M]^+$ (Supporting Information Figures S20 and S21).

HeQu-Ph: He-Ket (12.7 mg, 0.031 mmol) and compound **14** (10.5 mg, 0.040 mmol) were dissolved in acetic acid (2 mL) and $CHCl_3$ (10 mL) and the solution was stirred at 100 °C for 3 h. After 3 h, the solvent was evaporated. Next, flash column chromatography on silica gel with hexane/ethyl acetate (10/1 v/v) as eluent was carried out. Final purification was performed by preparative recycling gel permeation chromatography to afford HeQu-Ph as a yellow solid (13.3 mg, 0.021 mmol, 68 %). ^{1}H NMR (400 MHz, $CDCl_3$): $\delta = 9.55$ (d, $J = 8.3$ Hz, 2 H), 8.50 (s, 2 H), 8.16 (d, $J = 8.3$ Hz, 2 H), 7.74 (d, $J = 8.8$ Hz, 2 H), 7.50 (d, $J = 8.8$ Hz, 2 H), 7.37–7.34 (m, 12 H), 7.02–6.95 (m, 4 H), 6.46 ppm (dd, $J = 16.6$, 8.3 Hz, 2 H); ^{13}C NMR (100 MHz, $CDCl_3$): $\delta = 143.3$, 143.1, 140.6, 133.5, 131.7, 130.5, 130.1, 129.7, 129.5, 129.2, 128.5, 128.5, 128.2, 128.1, 127.2, 126.6, 125.7, 125.4, 124.9, 123.7, 122.9 ppm; MALDI-TOF MS: $m/z = 631$ $[M-H]^+$ (Supporting Information Figures S26 and S27).

HeQu-Ani: He-Ket (26.0 mg, 0.064 mmol) and compound **15** (15.5 mg, 0.048 mmol) were dissolved in acetic acid (2 mL) and EtOH (4 mL) and the solution stirred at 100 °C for 3 h. After cooling, the reaction mixture was filtered, and the solid was washed with EtOH and Et_2O. Then, the solid was dissolved in CH_2Cl_2 and the solvent was evaporated. Flash column chromatography on silica gel with hexane/ethyl acetate (1/1 v/v) as eluent afforded the crude product. Washing with hexane and solvent evaporation afforded the product HeQu-Ani as a yellow solid (27.3 mg, 0.039 mmol, 62 %). ^{1}H NMR (400 MHz, $CDCl_3$): $\delta = 9.53$ (d, $J = 8.3$ Hz, 2 H), 8.43 (s, 2 H), 8.14 (d, $J = 8.3$ Hz, 2 H), 7.73 (d, $J = 8.8$ Hz, 2 H), 7.49 (d, $J = 8.5$ Hz, 2 H), 7.33–7.29 (m, 6 H), 7.01–6.94 (m, 4 H), 6.89 (dd, $J = 6.7$, 2.0 Hz, 4 H), 6.45 (dd, $J = 16.6$, 8.3 Hz, 2 H), 3.86 ppm (s, 6 H); ^{13}C NMR (100 MHz, $CDCl_3$): $\delta = 143.0$, 142.9, 133.5, 133.1, 131.7, 131.2, 130.1, 129.8, 129.5, 129.2, 128.4, 128.2, 126.6, 125.7, 125.4, 125.0, 123.7, 122.9, 113.6, 55.3 ppm; MALDI-TOF MS: $m/z = 693$ $[M+H]^+$ (Supporting Information Figure S28 and S29).

HeQu-C$_{16}$: He-Ket (13.2 mg, 0.032 mmol) and compound **16** (23.8 mg, 0.040 mmol) were dissolved in acetic acid (5 mL), EtOH (5 mL), and CH_2Cl_2 (5 mL) and the solution stirred at 100 °C for 1 h. After cooling, the reaction mixture was filtered, and the solid was washed with water. After dissolving in CH_2Cl_2 and solvent evaporation, the product HeQu-C$_{16}$ was obtained as a yellow solid (22.8 mg, 0.020 mmol, 63 %). ^{1}H NMR (400 MHz, $CDCl_3$): $\delta = 9.42$ (d, $J = 8.3$ Hz, 2 H), 8.32(s, 2 H), 8.03 (d, $J = 8.3$ Hz, 2 H), 7.64 (d, $J = 8.8$ Hz, 2 H), 7.41 (d, $J = 8.3$ Hz, 2 H), 7.22 (d, $J = 8.3$ Hz, 6 H), 6.93–6.86 (m, 4 H), 6.80 (d, $J = 8.8$ Hz, 4 H), 6.37 (dd, $J = 7.6$, 3.8 Hz, 2 H), 3.92 (t, $J = 6.6$ Hz, 4 H), 1.75–1.72 (m, 4 H), 1.42–1.39 (m, 4 H), 1.20–1.20 (m, 48 H), 0.81 ppm (t, $J = 6.8$ Hz, 6 H); ^{13}C NMR (100 MHz, $CDCl_3$): $\delta = 158.4$, 143.0, 142.7, 141.5, 133.4, 132.9, 131.7, 131.1, 130.0, 129.7, 129.5, 129.2, 128.3, 128.1, 126.6, 125.6, 125.3, 124.9, 123.6, 122.8, 114.1, 68.0, 31.9, 29.7, 29.6, 29.5, 29.4, 26.1, 22.7, 14.1 ppm; MALDI-TOF MS: $m/z = 1114$ $[M+H]^+$ (Supporting Information Figures S30 and S31).

Electrochemical measurements

Cyclic voltammograms were recorded on an Iviumstat 20 V/2.5 A potentiostat by using a three-electrode system. A platinum electrode was used as the working electrode, a platinum wire as the counter electrode, and a saturated calomel electrode as reference electrode. Ferrocene/ferrocenium redox couple was used as internal standard. All solutions were purged wit hnitrogen gas prior to electrochemical measurements.

Spectroscopic measurements

UV/Vis absorption spectra were recorded on a PerkinElmer Lamda 750 UV/VIS/NIR spectrophotometer. CD spectra were recorded on Jasco J-820 instrument. Fluorescence spectra were recorded on PerkinElmer LS-55 spectrofluorophotometer. The absolute fluorescence quantum yields were measured with a Hamamatsu Photonics C9920-02 system equipped with an integrating sphere and a red-sensitive multichannel photodetector (PMA-12) at an excitation wavelength of 330 nm. Fluorescence lifetimes were measured on a Hamamatsu photonics C5680 with laser light (Hamamatsu photonics M10360, laser diode head, 390 nm) as excitation source.

Preparation of single crystals and structure analysis

Single crystals of *rac*-HeQu and *rac*-HeQu-Ani for were prepared by vapor diffusion of $CHCl_3$ into MeOH solutions at room temperature. Those of *P*-HeQu-Ani and *rac*-HeQu-Ph were prepared by vapor diffusion of 1,2-dichloroethane into MeOH solutions at room temperature. Crystal structure analysis was carried out on a Rigaku R-AXIS RAPID diffractometer with graphite-monochromated $Mo_{K\alpha}$ radiation. The structures were solved by direct methods (SHELXS-97). CCDC 982754, 982755, 982756 and 982757 contain the supplementary crystallographic data for this paper. These data can be obtained free of charge from The Cambridge Crystallographic Data Centre via www.ccdc.cam.ac.uk/data_request/cif.

Transmission electron microscopy

TEM measurements were performed on Tecnai Spirit (FEI Company) by applying a drop of 20 μM HeQu-C$_{16}$ in methylcyclohexane to a copper TEM grid. TEM images were recorded at an accelerating voltage of 120 kV.

Acknowledgements

This work was partially supported by Grant-in-Aid for Scientific Research (Nos. 23108721 & 23681025 to T.H.), MEXT-Supported Program for the Strategic Research Foundation at Private Universities, 2009–2013, and Mitsubishi Foundation. We are grateful to Mr. Shohei Katao (NAIST) for single-crystal X-ray diffraction analysis.

Keywords: electrochemistry · fluorescence · helical structures · stacking interactions · supramolecular chemistry

[1] a) L. Pauling, R. B. Corey, H. R. Branson, *Proc. Natl. Acad. Sci. USA* **1951**, *37*, 205 – 211; b) J. D. Watson, F. H. C. Crick, *Nature* **1953**, *171*, 737 – 738; c) T. Hahn, *Acta Crystallographica* **1958**, *11*, 825 – 825.

[2] a) M. Albrecht, E. Isaak, M. Baumert, V. Gossen, G. Raabe, R. Frohlich, *Angew. Chem.* **2011**, *123*, 2903 – 2906; *Angew. Chem. Int. Ed.* **2011**, *50*, 2850 – 2853; b) M. Kumar, N. Jonnalagadda, S. J. George, *Chem. Commun.* **2012**, *48*, 10948 – 10950; c) R. Glaser, *Chirality* **2008**, *20*, 910 –

918; d) T. Miyabe, H. Iida, M. Banno, T. Yamaguchi, E. Yashima, *Macromolecules* **2011**, *44*, 8687 – 8692; e) K. Kodama, Y. Kobayashi, K. Saigo, *Cryst. Growth Des.* **2007**, *7*, 935 – 939; f) K. Kodama, Y. Kobayashi, K. Saigo, *Chem. Eur. J.* **2007**, *13*, 2144 – 2152; g) H. Nakade, B. J. Jordan, H. Xu, G. Han, S. Srivastava, R. R. Arvizo, G. Cooke, V. M. Rotello, *J. Am. Chem. Soc.* **2006**, *128*, 14924 – 14929; h) A. Shchyrba, M. T. Nguyen, C. Wackerlin, S. Martens, S. Nowakowska, T. Ivas, J. Roose, T. Nijs, S. Boz, M. Schar, M. Stohr, C. A. Pignedoli, C. Thilgen, F. Diederich, D. Passerone, T. A. Jung, *J. Am. Chem. Soc.* **2013**, *135*, 15270 – 15273.

[3] a) R. M. Ho, M. C. Li, S. C. Lin, H. F. Wang, Y. D. Lee, H. Hasegawa, E. L. Thomas, *J. Am. Chem. Soc.* **2012**, *134*, 10974 – 10986; b) B. Willis, L. M. Eubanks, M. R. Wood, K. D. Janda, T. J. Dickerson, R. A. Lerner, *Proc. Natl. Acad. Sci. USA* **2008**, *105*, 1416 – 1419; c) R. Custelcean, D.-e. Jiang, B. P. Hay, W. Luo, B. Gu, *Cryst. Growth Des.* **2008**, *8*, 1909 – 1915; d) D. Chen, C. Zhu, H. Wang, J. E. Maclennan, M. A. Glaser, E. Korblova, D. M. Walba, J. A. Rego, E. A. Soto-Bustamante, N. A. Clark, *Soft Matter* **2013**, *9*, 462 – 471.

[4] a) S. Pieraccini, S. Bonacchi, S. Lena, S. Masiero, M. Montalti, N. Zaccheroni, G. P. Spada, *Org. Biomol. Chem.* **2010**, *8*, 774 – 781; b) F. Aparicio, F. Garcia, G. Fernandez, E. Matesanz, L. Sanchez, *Chem. Eur. J.* **2011**, *17*, 2769 – 2776; c) S. Shin, S. Lim, Y. Kim, T. Kim, T. L. Choi, M. Lee, *J. Am. Chem. Soc.* **2013**, *135*, 2156 – 2159; d) S. Manchineella, V. Prathyusha, U. D. Priyakumar, T. Govindaraju, *Chem. Eur. J.* **2013**, *19*, 16615 – 16624; e) C. T. Chen, C. H. Chen, T. G. Ong, *J. Am. Chem. Soc.* **2013**, *135*, 5294 – 5297; f) H.-G. Jin, X.-J. Hong, J. Li, Y.-Z. Yan, Y.-T. Liu, S.-H. Xu, Y.-P. Cai, *Dalton Trans.* **2012**, *41*, 14239 – 14243; g) C.-S. Chen, X.-D. Xu, S.-Y. Li, R.-X. Zhuo, X.-Z. Zhang, *Nanoscale* **2013**, *5*, 6270 – 6274; h) J. Wang, G. Yang, H. Jiang, G. Zou, Q. Zhang, *Soft Matter* **2013**, *9*, 9785 – 9791.

[5] a) K. Watanabe, H. Iida, K. Akagi, *Adv. Mater.* **2012**, *24*, 6451 – 6456; b) W. Z. Yuan, F. Mahtab, Y. Y. Gong, Z. Q. Yu, P. Lu, Y. H. Tang, J. W. Y. Lam, C. Z. Zhu, B. Z. Tang, *J. Mater. Chem.* **2012**, *22*, 10472 – 10479; c) R. J. Kumar, J. M. MacDonald, T. B. Singh, L. J. Waddington, A. B. Holmes, *J. Am. Chem. Soc.* **2011**, *133*, 8564 – 8573; d) H. Shao, T. Nguyen, N. C. Romano, D. A. Modarelli, J. R. Parquette, *J. Am. Chem. Soc.* **2009**, *131*, 16374 – 16376; e) L. Chen, K. S. Mali, S. R. Puniredd, M. Baumgarten, K. Parvez, W. Pisula, S. De Feyter, K. Mullen, *J. Am. Chem. Soc.* **2013**, *135*, 13531 – 13537.

[6] D. J. Hill, M. J. Mio, R. B. Prince, T. S. Hughes, J. S. Moore, *Chem. Rev.* **2001**, *101*, 3893 – 4012.

[7] J. W. Lam, B. Z. Tang, *Acc. Chem. Res.* **2005**, *38*, 745 – 754.

[8] a) K. Watanabe, I. Osaka, S. Yorozuya, K. Akagi, *Chem. Mater.* **2012**, *24*, 1011 – 1024; b) B. Narayan, C. Kulkarni, S. J. George, *J. Mater. Chem. C* **2013**, *1*, 626; c) S. Yagai, M. Yamauchi, A. Kobayashi, T. Karatsu, A. Kitamura, T. Ohba, Y. Kikkawa, *J. Am. Chem. Soc.* **2012**, *134*, 18205 – 18208; d) A. S. D. Sandanayaka, Y. Araki, T. Wada, T. Hasobe, *J. Phys. Chem. C* **2008**, *112*, 19209 – 19216; e) F. D'Souza, O. Ito, *Chem. Soc. Rev.* **2012**, *41*, 86 – 96.

[9] a) J. Lu, L. Wu, J. Jiang, X. Zhang, *Eur. J. Inorg. Chem.* **2010**, *2010*, 4000 – 4008; b) C. Zhao, B. Bai, H. Wang, S. Qu, G. Xiao, T. Tian, M. Li, *J. Mol. Struct.* **2013**, *1037*, 130 – 135.

[10] a) Y. Huang, J. Hu, W. Kuang, Z. Wei, C. F. J. Faul, *Chem. Commun.* **2011**, *47*, 5554 – 5556; b) X. Lu, Z. Guo, C. Sun, H. Tian, W. Zhu, *J. Phys. Chem. B* **2011**, *115*, 10871 – 10876; c) M. Banno, T. Yamaguchi, K. Nagai, C. Kaiser, S. Hecht, E. Yashima, *J. Am. Chem. Soc.* **2012**, *134*, 8718 – 8728; d) S. J. George, R. de Bruijn, Ž. Tomović, B. Van Averbeke, D. Beljonne, R. Lazzaroni, A. P. H. J. Schenning, E. W. Meijer, *J. Am. Chem. Soc.* **2012**, *134*, 17789 – 17796; e) T. Sasaki, I. Hisaki, T. Miyano, N. Tohnai, K. Morimoto, H. Sato, S. Tsuzuki, M. Miyata, *Nat. Commun.* **2013**, *4*, 1787.

[11] a) J. R. Aldrich-Wright, *Nat. Chem.* **2011**, *4*, 10 – 11; b) L. Aboshyan-Sorgho, M. Cantuel, G. Bernardinelli, C. Piguet, *Dalton Trans.* **2012**, *41*, 7218 – 7226; c) Y. Shinozaki, G. Richards, K. Ogawa, A. Yamano, K. Ohara, K. Yamaguchi, S.-i. Kawano, K. Tanaka, Y. Araki, T. Wada, J. Otsuki, *J. Am. Chem. Soc.* **2013**, *135*, 5262 – 5265; d) Y. Wei, K. Wu, J. He, W. Zheng, X. Xiao, *CrystEngComm* **2011**, *13*, 52 – 54; e) T. Grancha, C. Tourbillon, J. Ferrando-Soria, M. Julve, F. Lloret, J. Pasan, C. Ruiz-Perez, O. Fabelo, E. Pardo, *CrystEngComm* **2013**, *15*, 9312 – 9315; f) T. Sakuma, H. Sakai, T. Hasobe, *Chem. Commun.* **2012**, *48*, 4441 – 4443; g) T. Hasobe, H. Sakai, K. Mase, K. Ohkubo, S. Fukuzumi, *J. Phys. Chem. C* **2013**, *117*, 4441 – 4449.

[12] a) T. Hasobe, *J. Phys. Chem. Lett.* **2013**, *4*, 1771 – 1780; b) T. Hasobe, *Phys. Chem. Chem. Phys.* **2012**, *14*, 15975 – 15987; c) T. Hasobe, *Phys. Chem. Chem. Phys.* **2010**, *12*, 44 – 57.

[13] a) M. Sugino, Y. Araki, K. Hatanaka, I. Hisaki, M. Miyata, N. Tohnai, *Cryst. Growth Des.* **2013**, *13*, 4986 – 4992; b) Z. Zhao, S. Chen, J. W. Y. Lam, Z. Wang, P. Lu, F. Mahtab, H. H. Y. Sung, I. D. Williams, Y. Ma, H. S. Kwok, B. Z. Tang, *J. Mater. Chem.* **2011**, *21*, 7210 – 7216; c) Y. Sonoda, M. Goto, S. Tsuzuki, N. Tamaoki, *J. Phys. Chem. A* **2007**, *111*, 13441 – 13451; d) C. Yuan, S. Saito, C. Camacho, S. Irle, I. Hisaki, S. Yamaguchi, *J. Am. Chem. Soc.* **2013**, *135*, 8842 – 8845; e) J. Chen, A. Neels, K. M. Fromm, *Chem. Commun.* **2010**, *46*, 8282 – 8284; f) G. Zhang, G. Yang, S. Wang, Q. Chen, J. S. Ma, *Chem. Eur. J.* **2007**, *13*, 3630 – 3635; g) T. Seko, K. Ogura, Y. Kawakami, H. Sugino, H. Toyotama, J. Tanaka, *Chem. Phys. Lett.* **1998**, *291*, 438 – 444; h) T. Hinoue, Y. Shigenoi, M. Sugino, Y. Mizobe, I. Hisaki, M. Miyata, N. Tohnai, *Chem. Eur. J.* **2012**, *18*, 4634 – 4643; i) M. A. Fourati, T. Maris, W. G. Skene, C. G. Bazuin, R. E. Prud'homme, *J. Phys. Chem. B* **2011**, *115*, 12362 – 12369; j) L. Wang, W. Li, J. Lu, Y.-X. Zhao, G. Fan, J.-P. Zhang, H. Wang, *J. Phys. Chem. C* **2013**, *117*, 26811 – 26820; k) K. Nagura, S. Saito, H. Yusa, H. Yamawaki, H. Fujihisa, H. Sato, Y. Shimoikeda, S. Yamaguchi, *J. Am. Chem. Soc.* **2013**, *135*, 10322 – 10325.

[14] a) R. H. Martin, *Angew. Chem.* **1974**, *86*, 727 – 738; *Angew. Chem. Int. Ed. Engl.* **1974**, *13*, 649 – 660; b) T. Caronna, M. Catellani, S. Luzzati, L. Malpezzi, S. V. Meille, A. Mele, C. Richter, R. Sinisi, *Chem. Mater.* **2001**, *13*, 3906 – 3914.

[15] a) J. E. Field, G. Muller, J. P. Riehl, D. Venkataraman, *J. Am. Chem. Soc.* **2003**, *125*, 11808 – 11809; b) Y. Nakai, T. Mori, Y. Inoue, *J. Phys. Chem. A* **2012**, *116*, 7372 – 7385; c) Y. Sawada, S. Furumi, A. Takai, M. Takeuchi, K. Noguchi, K. Tanaka, *J. Am. Chem. Soc.* **2012**, *134*, 4080 – 4083.

[16] M. Sapir, E. V. Donckt, *Chem. Phys. Lett.* **1975**, *36*, 108 – 110.

[17] a) R. Carr, N. H. Evans, D. Parker, *Chem. Soc. Rev.* **2012**, *41*, 7673 – 7686; b) J. P. Riehl, F. S. Richardson, *Chem. Rev.* **1986**, *86*, 1 – 16; c) T. Harada, H. Tsumatori, K. Nishiyama, J. Yuasa, Y. Hasegawa, T. Kawai, *Inorg. Chem.* **2012**, *51*, 6476 – 6485; d) J. Kumar, T. Nakashima, H. Tsumatori, T. Kawai, *J. Phys. Chem. Lett.* **2014**, *5*, 316 – 321; e) H. Maeda, Y. Bando, K. Shimomura, I. Yamada, M. Naito, K. Nobusawa, H. Tsumatori, T. Kawai, *J. Am. Chem. Soc.* **2011**, *133*, 9266 – 9269.

[18] a) J. C. Dewan, *Acta Crystallogr.* **1981**, *37*, 1421 – 1424; b) M. Joly, N. Defay, R. H. Martin, J. P. Declerq, G. Germain, B. Soubrier-Payen, M. Van Meerssche, *Helv. Chim. Acta* **1977**, *60*, 537 – 560; c) R. Kuroda, *J. Chem. Soc. Perkin Trans. 2* **1982**, 789 – 794; d) M. K. Lakshman, P. L. Kole, S. Chaturvedi, J. H. Saugier, H. J. C. Yeh, J. P. Glusker, H. L. Carrell, A. K. Katz, C. E. Afshar, W. M. Dashwood, G. Kenniston, W. M. Baird, *J. Am. Chem. Soc.* **2000**, *122*, 12629 – 12636.

[19] K. Nakano, H. Oyama, Y. Nishimura, S. Nakasako, K. Nozaki, *Angew. Chem.* **2012**, *124*, 719 – 723; *Angew. Chem. Int. Ed.* **2012**, *51*, 695 – 699.

[20] a) T. Hatakeyama, S. Hashimoto, T. Oba, M. Nakamura, *J. Am. Chem. Soc.* **2012**, *134*, 19600 – 19603; b) M. Miyasaka, A. Rajca, M. Pink, S. Rajca, *J. Am. Chem. Soc.* **2005**, *127*, 13806 – 13807; c) E. Murguly, R. McDonald, N. R. Branda, *Org. Lett.* **2000**, *2*, 3169 – 3172.

[21] A. Rajca, M. Miyasaka, M. Pink, H. Wang, S. Rajca, *J. Am. Chem. Soc.* **2004**, *126*, 15211 – 15222.

[22] H. J. Son, W. S. Han, D. H. Yoo, K. T. Min, S. N. Kwon, J. Ko, S. O. Kang, *J. Org. Chem.* **2009**, *74*, 3175 – 3178.

[23] a) X.-K. Chen, J.-F. Guo, L.-Y. Zou, A.-M. Ren, J.-X. Fan, *J. Phys. Chem. C* **2011**, *115*, 21416 – 21428; b) K. E. Maly, *Cryst. Growth Des.* **2011**, *11*, 5628 – 5633.

[24] D. C. Harrowven, I. L. Guy, L. Nanson, *Angew. Chem.* **2006**, *118*, 2300 – 2303; *Angew. Chem. Int. Ed.* **2006**, *45*, 2242 – 2245.

[25] G.-S. Liou, H.-Y. Lin, *Eur. Polym. J.* **2006**, *42*, 1051 – 1058.

[26] L. RulíŠek, O. Exner, L. Cwiklik, P. Jungwirth, I. Starý, L. PospíŠil, Z. Havlas, *J. Phys. Chem. C* **2007**, *111*, 14948 – 14955.

[27] M. J. Fuchter, M. Weimar, X. Yang, D. K. Judge, A. J. P. White, *Tetrahedron Lett.* **2012**, *53*, 1108 – 1111.

[28] E. Vander Donckt, J. Nasielski, J. R. Greenleaf, J. B. Birks, *Chem. Phys. Lett.* **1968**, *2*, 409 – 410.

[29] J. B. Birks, D. J. S. Birch, E. Cordemans, E. Vander Donckt, *Chem. Phys. Lett.* **1976**, *43*, 33 – 36.

[30] N. J. Turro, *Modern Molecular Photochemistry*, University Science Books, Sausalito, **1991**, pp. 105 – 109.

[31] M. J. Frisch, G. W. Trucks, H. B. Schlegel, G. E. Scuseria, M. A. Robb, J. R. Cheeseman, J. Montgomery, J. A., T. Vreven, K. N. Kudin, J. C. Burant, J. M. Millam, S. S. Iyengar, J. Tomasi, V. Barone, B. Mennucci, M. Cossi, G. Scalmani, N. Rega, G. A. Petersson, H. Nakatsuji, M. Hada, M. Ehara, K. Toyota, R. Fukuda, J. Hasegawa, M. Ishida, T. Nakajima, Y. Honda, O.

Kitao, H. Nakai, M. Klene, X. Li, J. E. Knox, H. P. Hratchian, J. B. Cross, V. Bakken, C. Adamo, J. Jaramillo, R. Gomperts, R. E. Stratmann, O. Yazyev, A. J. Austin, R. Cammi, C. Pomelli, J. W. Ochterski, P. Y. Ayala, K. Morokuma, G. A. Voth, P. Salvador, J. J. Dannenberg, V. G. Zakrzewski, S. Dapprich, A. D. Daniels, M. C. Strain, O. Farkas, D. K. Malick, A. D. Rabuck, K. Raghavachari, J. B. Foresman, J. V. Ortiz, Q. Cui, A. G. Baboul, S. Clifford, J. Cioslowski, B. B. Stefanov, G. Liu, A. Liashenko, P. Piskorz, I. Komaromi, R. L. Martin, D. J. Fox, T. Keith, M. A. Al-Laham, C. Y. Peng, A. Nanayakkara, M. Challacombe, P. M. W. Gill, B. Johnson, W. Chen, M. W. Wong, C. Gonzalez, and J. A. Pople in Gaussian03, Gaussian Inc., Wallingford, CT, **2004**.

Received: February 28, 2014